energies

MDPI

Article

Coordinated Wind–Storage Frequency Regulation Strategy for Suppressing Frequency Fluctuations

Zengyao Tian [1], Chunshan Li [1], Rui Sun [2,*], Yang Liu [1], Kexin Li [2], Xiaotian Zhang [1], Mo Zhou [1], Junwen Dai [1] and Tianmeng Yang [1]

[1] NorthEast Branch of State Grid Corporation of China, Shenyang 110180, China; tianzengyao@ne.sgcc.com.cn (Z.T.); lichunshan@ne.sgcc.com.cn (C.L.)
[2] School of Electrical Engineering, Northeast Electric Power University, Jilin 132012, China
* Correspondence: sr1774385827@163.com

Abstract

With increasing renewable energy penetration, maintaining active power balance in power systems has become increasingly challenging. Repeated frequency crossings of the primary frequency regulation deadband may degrade frequency quality and shorten the service life of frequency regulation resources. To address this problem, a coordinated wind–storage frequency regulation strategy is proposed to suppress frequency fluctuations. First, a deadband boundary crossing model and evaluation metrics are developed to characterize crossing severity, crossing count, and repeated boundary switching. Second, a risk prediction method combining frequency deviation, rate of change of frequency, and short-term frequency forecasts is proposed to identify potential crossing periods. Based on the predicted risk, a hierarchical coordinated control strategy considering resource suitability is designed. Supercapacitor energy storage preferentially suppresses short-term fluctuations when the frequency approaches the deadband boundary, whereas wind turbines and energy storage jointly provide frequency regulation after the frequency deviation crosses the deadband boundary. Case studies demonstrate that the proposed strategy improves frequency quality, appropriately allocates frequency regulation duties among system resources, and reduces the overall operating cost.

Keywords: frequency fluctuation; wind–storage coordination; frequency regulation control; frequency regulation deadband

1. Introduction

Increasing penetration of wind, photovoltaic (PV), and other renewable sources challenges power-system active power balance [1,2]. Declining aggregate frequency-response capability increases system sensitivity to active power disturbances [3], while frequent renewable generation fluctuations disrupt this balance, causing greater frequency fluctuations during normal operation than in conventional systems [4].

Primary frequency regulation (PFR) typically incorporates a deadband to avoid frequent responses to minor disturbances [5]. Under high renewable penetration, frequency may remain within operational limits yet repeatedly cross PFR deadband boundaries, frequently activating and deactivating regulation resources, degrading frequency quality, and shortening their service life. In conventional generating units, frequent PFR operation increases movements of steam valves, guide vanes, and associated actuators, accelerating mechanical wear [6]. Frequent wind turbine participation may induce torque fluctuations

Check for updates

Academic Editor: Gabriele Discepoli

Received: 11 September 2026
Revised: 26 October 2026
Accepted: 5 November 2026
Published: 7 November 2026

Copyright: © 2026 by the authors. Licensee MDPI, Basel, Switzerland. This article is an open access article distributed under the terms and conditions of the Creative Commons Attribution (CC BY) license.

and increase mechanical loads, reducing fatigue life [7]. Despite their rapid response, energy storage systems subjected to prolonged high-frequency, small-amplitude bidirectional regulation experience more charge–discharge transitions and equivalent full cycles, shortening battery life and reducing usable capacity [8].

Research on frequency regulation in power systems with high renewable penetration generally falls into four categories. The first examines how renewable integration affects system frequency characteristics. Ref. [9] investigates the impacts of system inertia, primary frequency regulation (PFR) reserve, and PFR ramping rate on frequency stability. Ref. [10] accounts for uncertainties in renewable energy generation and load demand, proposes frequency stability indicators, and assesses the inertial support requirements under different renewable energy penetration levels. Ref. [11] employs eigenvalue and sensitivity analyses to quantify the impacts of renewable energy penetration on the rate of change of frequency (RoCoF), frequency nadir, and system stability. These studies mainly address unit trips and other large generation deficits, with limited attention to persistent fluctuations caused by stochastic renewable generation, particularly repeated PFR deadband boundary crossings.

The second investigates wind-power participation through virtual inertia control [12], primary frequency control [13], overspeed control [14], and pitch-angle control [15]. Appropriately designed strategies improve system frequency response and reduce deviations. However, wind-turbine regulation capability is constrained by wind speed and de-loading level, among other factors, making available capacity time-varying [16–18].

The third addresses energy-storage participation. Ref. [19] incorporates the state of charge (SOC) into a hierarchical frequency regulation scheme to coordinate frequency restoration with charging and discharging constraints. Ref. [20] proposes a distributed frequency regulation strategy for multiple energy storage systems, while accounting for operating costs, frequency regulation requirements, and uncertainties in renewable energy generation.

The fourth investigates coordinated wind–storage regulation to improve frequency performance and reduce individual resource burdens. Ref. [21] proposes a coordinated frequency regulation strategy in which wind power provides the primary regulation response and the energy storage system compensates for the remaining regulation error. The proposed strategy improves frequency regulation accuracy without compromising battery lifetime. Ref. [22] develops a hierarchical model predictive control (MPC) strategy to coordinate the power outputs of the wind farm and battery energy storage system, thereby reducing the maximum frequency deviation and improving SOC recovery. Ref. [23] proposes a coordinated wind–storage primary frequency regulation strategy with variable control coefficients determined by wind speed and SOC, which improves the frequency nadir, reduces the number of battery frequency regulation actions, and alleviates the regulation burden that would otherwise be borne solely by the energy storage system. Nevertheless, most studies emphasize improving the frequency nadir and reducing maximum frequency deviation, with insufficient attention to frequent resource activation caused by repeated crossings near PFR deadband boundaries.

Complementary to studies on frequency response and coordinated regulation, recent research has also advanced wind speed forecasting. Ref. [24] proposed a stacked hybrid framework combining artificial neural networks, support vector regression, and random forest regression for one-hour-ahead wind speed forecasting. Such forecasting advances can inform wind power scheduling and reserve allocation. However, wind speed forecasting and short-term frequency trend prediction address different variables and time scales. The present study focuses on the latter by combining frequency deviation, the rate of change of frequency (RoCoF), and short-term frequency forecasts to identify PFR deadband boundary crossing risks and enable preemptive coordinated wind–storage frequency regulation.

To address these issues, this paper investigates frequency fluctuations in power systems with a high penetration of renewable energy, with particular emphasis on the repeated crossing of PFR deadband boundaries. A coordinated wind–storage frequency-regulation strategy for suppressing frequency fluctuations is proposed. The main contributions are summarized as follows:

(1) A model of the PFR deadband crossing process is established. Evaluation metrics are developed in terms of the magnitude of excursions beyond the deadband boundaries, the number of boundary crossings, and the characteristics of repeated switching between the inside and outside of the deadband. These metrics enable a quantitative characterization of repeated frequency crossings near the PFR deadband boundaries.

(2) A frequency-feature-based activation rule is developed for preemptive supercapacitor support. Filtered RoCoF is used for short-term frequency trend extrapolation, and the current and extrapolated frequency deviations are combined into a normalized crossing-risk signal. This signal determines the activation level of supercapacitor support while the current frequency deviation remains within the PFR deadband.

(3) A hierarchical coordinated wind–storage frequency regulation strategy tailored to the operating characteristics of different resources is proposed. Based on the rapid response capability of supercapacitor energy storage and the regulation constraints of wind turbines, a hierarchical coordination mechanism is designed. During the deadband-crossing risk stage, the supercapacitor is preferentially utilized to suppress short-term frequency fluctuations. Once the frequency actually crosses a deadband boundary, wind power and energy storage are coordinated to provide joint frequency regulation. The proposed strategy therefore reduces the frequent activation and deactivation of frequency-regulation resources while improving the cost-effectiveness of frequency regulation.

2. Modeling and Evaluation Metrics for Primary Frequency Regulation Deadband Boundary Crossings

2.1. Modeling of Primary Frequency Regulation Deadband Boundary Crossings

Let f_0 denote the nominal system frequency and $f(t)$ the instantaneous grid frequency. The frequency deviation $\Delta f(t)$ is then defined as given in (1).

$$\Delta f(t) = f(t) - f_0 \tag{1}$$

Let Δf_{db} denote the width of the primary frequency regulation deadband and the half-width of the primary frequency regulation (PFR) deadband. The frequency deviation within the deadband satisfies the condition given in (2).

$$|\Delta f(t)| \le \Delta f_{\mathrm{db}} \tag{2}$$

To characterize the nonlinear behavior of the primary frequency regulation deadband, a deadband function is defined as given in (3).

$$\varphi(\Delta f(t)) = \begin{cases} 0, & |\Delta f(t)| \le \Delta f_{\mathrm{db}} \\ \Delta f(t) - \mathrm{sgn}(\Delta f(t))\Delta f_{\mathrm{db}}, & |\Delta f(t)| > \Delta f_{\mathrm{db}} \end{cases} \tag{3}$$

where $\mathrm{sgn}(\cdot)$ denotes the signum function. When $|\Delta f(t)| \le \Delta f_{\mathrm{db}}$, $\varphi(\Delta f(t)) = 0$, indicating that the frequency deviation remains within the deadband and the frequency-regulation resources remain inactive. When $|\Delta f(t)| > \Delta f_{\mathrm{db}}$, $\varphi(\Delta f(t)) \neq 0$, indicating that the frequency deviation has crossed the deadband boundary and the frequency regulation resources are activated. Here $|\varphi(\Delta f(t))|$ represents the effective frequency deviation beyond the deadband boundary.

As can be seen from (3), the deadband function introduces pronounced piecewise nonlinearity into primary frequency regulation control. When the frequency deviation fluctuates repeatedly near the deadband boundary, the output of the deadband function switches frequently between zero and nonzero values, resulting in the repeated activation and deactivation of frequency regulation resources.

Grid frequency is fundamentally determined by the active power imbalance. For an equivalent system incorporating conventional frequency regulation resources, wind power frequency regulation, and energy storage frequency regulation, the frequency dynamics can be expressed as follows.

$$\frac{2H}{f_0}\frac{d\Delta f(t)}{dt} = \Delta P_{\mathrm{g}}(t) + \Delta P_{\mathrm{w}}(t) + \Delta P_{\mathrm{es}}(t) - \Delta P_{\mathrm{L}}(t) - \Delta P_{\mathrm{re}}(t) - D\Delta f(t) \tag{4}$$

where H is the equivalent inertia constant of the system; D is the system damping coefficient; $\Delta P_{\mathrm{g}}(t)$, $\Delta P_{\mathrm{w}}(t)$, and $\Delta P_{\mathrm{es}}(t)$ denote the primary frequency regulation power provided by conventional resources, wind power, and the energy storage system, respectively; $\Delta P_{\mathrm{re}}(t)$ represents fluctuations in renewable power generation; and $\Delta P_{\mathrm{L}}(t)$ represents load variations.

Equation (4) indicates that the frequency deviation is jointly affected by power disturbances, system inertia, damping, and the response capabilities of frequency regulation resources. With a high penetration of renewable energy, increasingly pronounced stochastic fluctuations in wind and photovoltaic power generation exacerbate the active power imbalance. Meanwhile, the reduction in system inertia makes the grid frequency more sensitive to power disturbances and, consequently, more likely to approach or cross the frequency regulation deadband boundaries. Therefore, frequency regulation deadband boundary crossings result from the combined effects of stochastic renewable power fluctuations and reduced system inertia.

2.2. Evaluation Metrics for Frequency Regulation Deadband Boundary Crossings

For discretely sampled data, let $\varphi_k = \varphi(\Delta f(k))$, where $\Delta f(k)$ denotes the frequency deviation at the *kth* sampling instant, $k = 1, 2, \ldots, N$, and Δt denotes the sampling interval. The maximum deadband exceedance magnitude is used to quantify the largest frequency excursion beyond the frequency regulation deadband boundary.

$$A_{\mathrm{db}}^{\max} = \max_{1\le k\le N}|\varphi_k| \tag{5}$$

The deadband boundary crossing count quantifies the number of transitions of the frequency deviation from inside to outside the PFR deadband.

$$\begin{cases} N_{\mathrm{db}}^{+} = \sum_{k=2}^{N} I[\varphi_{k-1} = 0, \varphi_k > 0] \\ N_{\mathrm{db}}^{-} = \sum_{k=2}^{N} I[\varphi_{k-1} = 0, \varphi_k < 0] \\ N_{\mathrm{db}} = N_{\mathrm{db}}^{+} + N_{\mathrm{db}}^{-} \end{cases} \tag{6}$$

where $\mathrm{I}[\cdot]$ is the indicator function, which equals 1 when the condition in brackets is satisfied and 0 otherwise. N_{db}^{+} and N_{db}^{-} denote the numbers of crossings of the positive and negative deadband boundaries, respectively, and N_{db} is the total deadband boundary crossing count.

To quantify repeated switching between the inside and outside of the deadband, the deadband boundary switching intensity is defined as given in (7).

$$S_{\mathrm{db}} = \sum_{k=2}^{N}|I[|\varphi_k| > 0] - I[|\varphi_{k-1}| > 0]| \tag{7}$$

This metric compares the deadband states of two consecutive samples. A switch is counted whenever the state changes. A large $S_{db\mathrm{db}}$ indicates pronounced repeated crossings near the frequency regulation deadband boundaries.

Together, these metrics characterize deadband boundary crossings in terms of exceedance magnitude, crossing count, and repeated boundary switching. $A_{\mathrm{db}}^{\max}$ quantifies the maximum magnitude of a single excursion beyond the deadband, $N_{db\mathrm{db}}$ represents the number of times frequency regulation is triggered, and $S_{db\mathrm{db}}$ measures the intensity of repeated switching between the inside and outside of the deadband. In addition to the deadband exceedance magnitude, deadband boundary crossing count, and deadband boundary switching intensity, mean absolute error (MAE) and root mean square error (RMSE) are used to evaluate the frequency response over the complete simulation interval. MAE and RMSE quantify its average magnitude and overall error level, respectively.

3. Deadband Boundary Crossing Risk Prediction

Conventional primary frequency regulation (PFR) generally employs a post-crossing activation logic, whereby frequency regulation resources respond only after the frequency deviation crosses a PFR deadband boundary. In conventional power systems, this approach prevents the resources from responding frequently to minor frequency disturbances. However, in power systems with high renewable penetration, such a passive post-crossing response may cause frequent activation and deactivation of frequency regulation resources.

This paper adopts a strategy of prediction and suppression before deadband boundary crossing. The key idea is to determine whether the frequency deviation tends to cross a PFR deadband boundary based on the frequency deviation and the rate of change of frequency (RoCoF). Preemptive support is requested when the combined frequency risk magnitude defined below exceeds the warning threshold while the current frequency deviation remains within the PFR deadband. Additional wind turbine frequency support is enabled only after actual deadband exceedance.

The RoCoF can be calculated from the frequency deviations at two consecutive sampling instants as follows.

$$r_{\mathrm{f}}(k) = \frac{\Delta f(k) - \Delta f(k-1)}{\Delta t} \tag{8}$$

Because frequency measurements may contain noise, a first-order smoothing filter is applied to obtain a smoothed RoCoF and reduce the sensitivity of the RoCoF estimate to measurement noise.

$$\bar{r}_{\mathrm{f}}(k) = \beta \bar{r}_{\mathrm{f}}(k-1) + (1-\beta) r_{\mathrm{f}}(k) \tag{9}$$

where β is the filter coefficient. A larger β produces a smoother RoCoF estimate but results in a slower response, whereas a smaller β makes the RoCoF estimate more sensitive to short-term fluctuations.

The trend extrapolation based on the current frequency deviation and RoCoF.

$$\widehat{\Delta f}(k+\tau) = \Delta f(k) + \tau \bar{r}_{\mathrm{f}}(k) \tag{10}$$

where τ is the short-term prediction horizon.

Equation (10) indicates that, if the current frequency trend remains unchanged over the short prediction horizon, the frequency deviation at time t + τ is predicted to be $\widehat{\Delta f}(k+\tau)$. To enable preemptive control, a deadband warning threshold is introduced.

$$\Delta f_{\mathrm{th}} = \Delta f_{\mathrm{db}} - \varepsilon \tag{11}$$

where ε is the preemptive control margin satisfying $(0 < \varepsilon < \Delta f_{\mathrm{db}})$, such that the warning threshold lies within the PFR deadband. This threshold is applied to the combined frequency risk magnitude $\mathrm{Z}_f(\mathrm{k})$ defined in (12).

Based on the current and predicted frequency deviations, a combined frequency risk magnitude is defined.

$$Z_f(k) = \max\left(|\Delta f(k)|, \left|\widehat{\Delta f}(k+\tau)\right|\right) \tag{12}$$

The role of $Z_f(k)$ is twofold. When the current frequency deviation has crossed a deadband boundary, the regulating action is maintained even if the predicted deviation decreases as the frequency recovers. When the current frequency deviation remains within the deadband but the predicted deviation approaches a deadband boundary, the control strategy intervenes preemptively. Based on $Z_f(k)$, a normalized deadband boundary crossing risk index is defined.

$$R_{db}(k) = \max\left(\frac{Z_f(k) - \Delta f_{th}}{\varepsilon}, 0\right) \tag{13}$$

Equation (13) quantifies the normalized risk level associated with the combined frequency risk magnitude. Since $Z_f(k)$ accounts for both current and predicted frequency deviations, $R_{db}(k)$ represents the combined risk rather than an indicator of actual deadband exceedance.

A risk activation coefficient $\Gamma(k)$ is further defined to convert the deadband boundary crossing risk into frequency regulation intensity.

$$\Gamma(k) = \min(R_{db}(k), 1) \tag{14}$$

When $\Gamma(k) = 0$, no additional frequency support is requested. For $0 < \Gamma(k) < 1$, the supercapacitor response intensity increases with the risk level. When $\Gamma(k) = 1$, the current or predicted frequency deviation reaches or exceeds the deadband boundary, and the activation coefficient is saturated. This condition does not necessarily indicate actual exceedance. Wind turbine participation is determined separately by the current frequency deviation.

The warning margin γ and the RoCoF smoothing coefficient β are fixed parameters in this study. Increasing γ moves the warning threshold farther inside the PFR deadband and may initiate supercapacitor support earlier. Increasing β strengthens noise attenuation but slows RoCoF tracking.

4. Coordinated Wind–Storage Frequency Regulation Strategy Considering Resource Suitability

Suppressing frequency fluctuations near the PFR deadband does not necessarily reduce the total number of control actions performed by all frequency regulation resources. PFR is automatically activated once the frequency deviation crosses a deadband boundary, making the corresponding resource response unavoidable. Simply widening the deadband to reduce the number of control actions would decrease the sensitivity of frequency regulation, increase the frequency deviation, and adversely affect frequency stability. This study focuses on reducing the repeated activation and deactivation of frequency-regulation resources near PFR deadband boundaries without widening the deadband. Its performance is evaluated in terms of system frequency response and modeled operating cost. Accordingly, a risk activation signal is constructed from frequency deviation, filtered RoCoF, and short-term trend extrapolation to determine when preemptive supercapacitor support is requested. Hierarchical regulation is then implemented according to the characteristics of different resources.

4.1. Analysis of Resource Suitability for Frequency Regulation

Coordinated frequency regulation requires allocating tasks according to each resource's physical characteristics. To avoid sustained energy production losses, wind turbines generally operate in maximum power point tracking (MPPT) mode, with superimposed integrated virtual inertia control enabling rotor kinetic energy release for active power support

when the frequency deviation crosses a PFR deadband boundary. This support shifts rotor speed from its optimum, reducing wind energy capture if prolonged. Rotor speed recovery must be carefully managed to avoid secondary frequency fluctuations. To limit repeated wind-turbine adjustments in response to high-frequency, small-amplitude fluctuations, the proposed strategy prioritizes the supercapacitor for short-term support and coordinates wind-turbine participation after an actual PFR deadband crossing. This allocation may help moderate dynamic loading; its implications for turbine fatigue life can be further assessed using turbine-level torque and load histories.

Table 1 summarizes the key technical characteristics of several energy storage technologies. Pumped hydro storage and compressed air energy storage offer large storage capacities but have relatively long response times, making them more suitable for energy regulation over longer time scales. Lithium-ion batteries provide substantial energy support; however, their cycle life is relatively limited, making them unsuitable for sustained high frequency regulation near the deadband boundaries. Flywheel energy storage is a form of mechanical energy storage, and frequent regulation may still cause operational losses in its rotating mechanical components. By contrast, supercapacitors offer millisecond-scale response, high round-trip efficiency, and long cycle life. They are therefore well suited to short-duration, high-frequency, and low-energy power regulation tasks. These characteristics closely match the control requirements of the proposed strategy for the short-term preemptive suppression of high-frequency, small-amplitude fluctuations. Accordingly, supercapacitors are selected as the preferred energy storage resource for mitigating deadband boundary crossing risks before an actual crossing occurs in coordinated wind–storage frequency regulation.

Table 1. Types and key characteristics of energy storage.

Category		Power/MW	Capacity/MW·h	Response Time	Discharge Duration at Rated Power	Round Trip Efficiency/%	Cycle Life/Cycles
Mechanical Energy Storage	Pumped Hydro Storage	10~5000	1000~10^5	minutes	1~24 h	70~85	15,000~20,000
	Flywheel Energy Storage	0.001~5	0.025~5	4 ms~s	s~15 min	80~9 5	10^5~10^6
	Compressed Air Energy Storage	10~1000	200~4000	3~10 min	1~24 h	50~75	10,000
Electrochemical Energy Storage	Lithium Ion Battery	0.001~100	1~1000	ms to s	0.5~10 h	85~95	2000~10,000
	Lead Acid Battery	0.001~100	0.01~100	ms	s~5 h	70~85	>500
	Vanadium Redox Flow Battery	0.01~10	4~40	ms to s	4~10 h	60~75	13,000
	Sodium Sulfur Battery	0.001~10	8~245	ms tos	1~8 h	75~85	2000~5000
Electrical Energy Storage	Superconducting Magnetic Energy Storage	0.01~10	0.015~0.1	1~5 ms	ms to s	90~95	>10^5
	Supercapacitor	0.01~1	10^{-6}~0.02	1~20 ms	s~1 min	90~98	10^5~10^6

Hierarchical coordinated control leverages the complementary response speeds and energy-support capabilities of different frequency regulation resources. The supercapacitor energy storage system, characterized by fast response and high power density, compensates for transient active power imbalances at the onset of disturbances, thereby reducing the rate of change of frequency (RoCoF) and maximum frequency deviation. Slower-response resources provide sustained power support.

Previous studies have employed fast nonsingular terminal sliding mode (FNTSM) control to improve coordination speed and convergence in voltage–power coordinated

control. Although FNTSM is not directly adopted here, its concepts of multi-timescale coordination and rapid dynamic compensation provide a theoretical reference for the proposed hierarchical mechanism [25]. These concepts guide the allocation of frequency regulation power between the supercapacitor and other resources to suppress short-term frequency fluctuations and sustained active power imbalances. Based on time-scale separation and dynamic power balance, the proposed control procedure integrates deadband boundary crossing risk prediction, primary frequency regulation (PFR) deadband state identification, rapid supercapacitor power compensation, and SOC constraints.

4.2. Integrated Virtual Inertia Control of Wind Turbines

Integrated virtual inertia control incorporates both the RoCoF term and the frequency deviation term. According to ref. [16], the short-term upward regulation capability of wind power is expressed as follows.

$$P_{\mathrm{w}}^{\mathrm{up}}(k) = \frac{T_{\mathrm{j}}(\omega_{\mathrm{r}}^2(k) - \omega_{\mathrm{min}}^2)}{2T_{\mathrm{f}}\cos\varphi} - P_{\mathrm{loss}}^{\mathrm{up}}(k) \tag{15}$$

where T_{j} is the rotor inertia time constant; T_{f} is the average frequency regulation duration; $\cos\varphi$ is the power factor; $\omega_{\mathrm{MPPT}}(k)$ is the optimal rotor speed at the current wind speed; $\omega_{\mathrm{r}}(k)$ is the current rotor speed; and $P_{\mathrm{loss}}^{\mathrm{up}}(k)$ is the mechanical power loss caused by rotor deceleration away from the MPPT operating point.

$P_{\mathrm{loss}}^{\mathrm{up}}(k)$ can be calculated from (16).

$$P_{\mathrm{loss}}^{\mathrm{up}}(k) = \frac{(P_{\mathrm{MPPT}}(k) - P_{\mathrm{min}})(\omega_{\mathrm{r}}(k) - \omega_{\mathrm{MPPT}}(k))^2}{(\omega_{\mathrm{MPPT}}(k) - \omega_{\mathrm{min}})^2} \tag{16}$$

where ω_{min} is the minimum rotor speed; P_{min} is the power output corresponding to the minimum rotor speed; and $P_{\mathrm{MPPT}}(k)$ is the MPPT power output of the wind turbine at the current wind speed.

Similarly, the short-term downward regulation capability of wind power is expressed as follows:

$$P_{\mathrm{w}}^{\mathrm{down}}(k) = \frac{T_{\mathrm{j}}(\omega_{\mathrm{max}}^2 - \omega_r^2(k))}{2T_{\mathrm{f}}\cos\varphi} + P_{\mathrm{loss}}^{\mathrm{down}}(k) \tag{17}$$

$P_{\mathrm{loss}}^{\mathrm{down}}(k)$ arises because rotor acceleration causes the wind turbine to deviate from the MPPT operating point, thereby reducing the captured mechanical power and, consequently, the active power delivered to the grid. ω_{max} denote the maximum allowable rotor speeds of the wind turbine. $P_{\mathrm{loss}}^{\mathrm{down}}(k)$ can be calculated from (18).

$$P_{\mathrm{loss}}^{\mathrm{down}}(k) = \frac{(P_{\mathrm{MPPT}}(k) - P_{\mathrm{max}})(\omega_{\mathrm{r}}(k) - \omega_{\mathrm{MPPT}}(k))^2}{(\omega_{\mathrm{max}} - \omega_{\mathrm{MPPT}}(k))^2} \tag{18}$$

where ω_{max} is the maximum rotor speed, and P_{max} is the power output corresponding to the maximum rotor speed.

During the simulation, the wind-speed trajectory is supplied to the wind-turbine model at each time step. The MPPT power, optimal rotor speed, and available upward and downward regulation capacities are updated according to (15)–(18). The rotor speed is updated using the turbine rotor dynamic equation and is constrained by the specified rotor-speed limits. The wind-turbine rotor inertia time constant $\mathrm{T_j}$ is a turbine-side parameter, whereas the equivalent inertia constant H describes the system frequency response. They represent the rotor dynamics and the aggregate system frequency dynamics, respectively.

4.3. Supercapacitor Energy Storage System

Let $P_{\mathrm{sc}}(k)$ denote the output power of the supercapacitor. A positive value indicates discharging and active power injection into the system, whereas a negative value indicates

charging and active power absorption from the system. Its state of charge (SOC) is given by (19).

$$\begin{cases} \mathrm{SOC}_{sc}(k+1) = \mathrm{SOC}_{sc}(k) - \frac{P_{\mathrm{sc}}^{+}(k)\Delta t}{3600\eta_{\mathrm{sc}}^{\mathrm{dis}}E_{\mathrm{sc}}} + \frac{\eta_{\mathrm{sc}}^{\mathrm{ch}}P_{\mathrm{sc}}^{-}(k)\Delta t}{3600E_{\mathrm{sc}}} \\ P_{\mathrm{sc}}^{+}(k) = \max(P_{\mathrm{sc}}(k), 0) \\ P_{\mathrm{sc}}^{-}(k) = \max(-P_{\mathrm{sc}}(k), 0) \end{cases} \tag{19}$$

where E_{sc} is the rated energy capacity of the supercapacitor, and $\eta_{\mathrm{sc}}^{\mathrm{dis}}$ and $\eta_{\mathrm{sc}}^{\mathrm{ch}}$ are its discharge and charge efficiencies, respectively. P_{sc} is expressed in MW, Δt is converted to hours, and E_{sc} is expressed in MWh.

The supercapacitor is represented at the supervisory active-power level in the present system model. Converter switching and inner-loop power-tracking dynamics are not explicitly resolved. Recent research on variable-gain NTSM control for DC–DC buck converters which demonstrates the importance of converter dynamics under parameter perturbations [26]. That converter-level controller is not adopted here; consequently, the present results do not establish robustness to converter parameter variations.

4.4. Coordinated Wind–Storage Frequency Regulation Strategy

Based on the deadband boundary crossing risk prediction method developed above, a coordinated wind–storage frequency regulation strategy considering resource suitability is proposed. Before a deadband boundary crossing, the supercapacitor preferentially handles high-frequency, small-amplitude fluctuations because of its fast response and long cycle life, while the wind turbines remain in MPPT operation whenever possible. Once the frequency deviation crosses a PFR deadband boundary, the wind turbines participate in coordinated regulation within their rotor speed and power limits. This strategy reduces frequent wind turbine responses near the deadband boundaries, thereby limiting rotor speed deviations and mechanical stress. Meanwhile, the supercapacitor's rapid charging and discharging capability suppresses the tendency toward boundary crossing and reduces repeated crossings.

The operating state is determined jointly by the combined frequency risk magnitude $Z_{\mathrm{f}}(k)$ and the current frequency deviation $|\Delta f(k)|$. When $Z_{\mathrm{f}}(k) \le \Delta f_{\mathrm{th}}$, neither resource provides additional frequency support. When $Z_{\mathrm{f}}(k) > \Delta f_{\mathrm{th}}$ while $|\Delta f(k)| \le \Delta f_{\mathrm{db}}$, only the supercapacitor provides preemptive support according to $\Gamma(k)$. Additional wind turbine support remains disabled in this state, even if the predicted risk causes $\Gamma(k) = 1$. When $|\Delta f(k)| > \Delta f_{\mathrm{db}}$, the wind turbines and supercapacitor provide coordinated frequency regulation.

4.4.1. Supercapacitor Frequency Regulation Before Deadband Boundary Crossing

The supercapacitor provides frequency support according to the risk activation coefficient. The control law in (20) applies both before actual deadband exceedance, when preemptive support is required, and after exceedance during coordinated regulation. Its final output is subject to the power and SOC constraints in (21) and (22).

$$\Delta P_{\mathrm{sc}}(k) = -\Gamma(k)\left[K_{\mathrm{sc,f}}\Delta f(k) + K_{\mathrm{sc,r}}\bar{r}_{\mathrm{f}}(k)\right] \tag{20}$$

where $K_{\mathrm{sc,f}}$ and $K_{\mathrm{sc,r}}$ are the frequency deviation and RoCoF control gains of the supercapacitor, respectively. The supercapacitor injects positive active power when frequency is below nominal and falling, and absorbs active power when frequency is above nominal and rising, preventing further deviation from nominal frequency.

Considering the limited energy capacity of the supercapacitor, its actual frequency regulation power must satisfy both power and SOC constraints.

$$\begin{cases} -P_{\mathrm{sc}}^{\mathrm{ch.max}}(k) \le \Delta P_{\mathrm{sc}}(k) \le P_{\mathrm{sc}}^{\mathrm{dis.max}}(k) \\ \mathrm{SOC}_{\mathrm{sc}}^{\min} \le \mathrm{SOC}_{\mathrm{sc}}(k) \le \mathrm{SOC}_{\mathrm{sc}}^{\max} \end{cases} \tag{21}$$

where $P_{sc}^{ch.max}$ and $P_{sc}^{dis.max}$ denote the maximum charging and discharging power of the supercapacitor, respectively; SOC_{sc}^{min} and SOC_{sc}^{max} denote its upper and lower SOC limits, respectively.

4.4.2. Coordinated Wind–Storage Frequency Regulation After Deadband Boundary Crossing

Before deadband boundary crossing, the wind turbine does not participate in frequency regulation and remains in MPPT operation.

$$P_w(k) = P_{MPPT}(k) \tag{22}$$

After the frequency deviation crosses a PFR deadband boundary, the wind turbine participates in coordinated frequency regulation. The frequency regulation power command generated by its integrated virtual inertia controller is given by (23).

$$\Delta P_{w,vi}(k) = -\Gamma(k)\left[K_{w,f}\Delta f(k) + K_{w,r}\bar{r}_f(k)\right] \tag{23}$$

where $K_{w,f}$ and $K_{w,r}$ are the frequency deviation and RoCoF control gains of the wind turbine, respectively.

After providing frequency support, the rotor speed of the wind turbine deviates from its optimal value. To prevent a prolonged rotor speed deviation, rotor speed recovery control is required. The power command for rotor speed recovery is given by (24).

$$\Delta P_w^{rec}(k) = -(1-\Gamma(k))K_{rec}[\omega_{MPPT}(k) - \omega_r(k)] \tag{24}$$

where K_{rec} is the rotor speed recovery gain.

When the deadband boundary crossing risk is high, $\Gamma(k)$ is large, which suppresses rotor speed recovery and prevents the recovery process from interfering with frequency fluctuation mitigation. When the deadband boundary crossing risk is low, $\Gamma(k)$ is small, allowing the wind turbine to gradually restore its rotor speed.

Considering both integrated virtual inertia control and rotor speed recovery control, the frequency regulation power command of the wind turbine is given by (25).

$$\Delta P_w(k) = \Delta P_{w,vi}(k) + \Delta P_w^{rec}(k) \tag{25}$$

The frequency regulation power of the wind turbine is limited by the available rotor kinetic energy and rotor speed limits and must satisfy the corresponding constraints.

$$\begin{cases} \omega_{min} \le \omega_r(k) \le \omega_{max} \\ -P_w^{down}(k) \le \Delta P_w(k) \le P_w^{up}(k) \end{cases} \tag{26}$$

Combining the frequency regulation power contributions of the supercapacitor and the wind turbine, the coordinated wind–storage power output is given by (27).

$$\Delta P_{total}(k) = \Delta P_w(k) + \Delta P_{sc}(k) \tag{27}$$

Figure 1 illustrates the resource activation logic. Following frequency prediction and risk assessment, $Z_f(k) > \Delta f_{th}$ is first checked. If this condition is not satisfied, no additional frequency support is activated. Otherwise, the current frequency deviation is compared with the PFR deadband boundary. The supercapacitor provides preemptive support when $|\Delta f(k)| \le \Delta f_{db}$, whereas the wind turbines and supercapacitor provide coordinated regulation when $|\Delta f(k)| \le \Delta f_{db}$. The zero wind turbine command shown in the inactive branches refers to $\Delta P_{w,vi}(k)$; rotor speed recovery is described separately by (24) and (25).

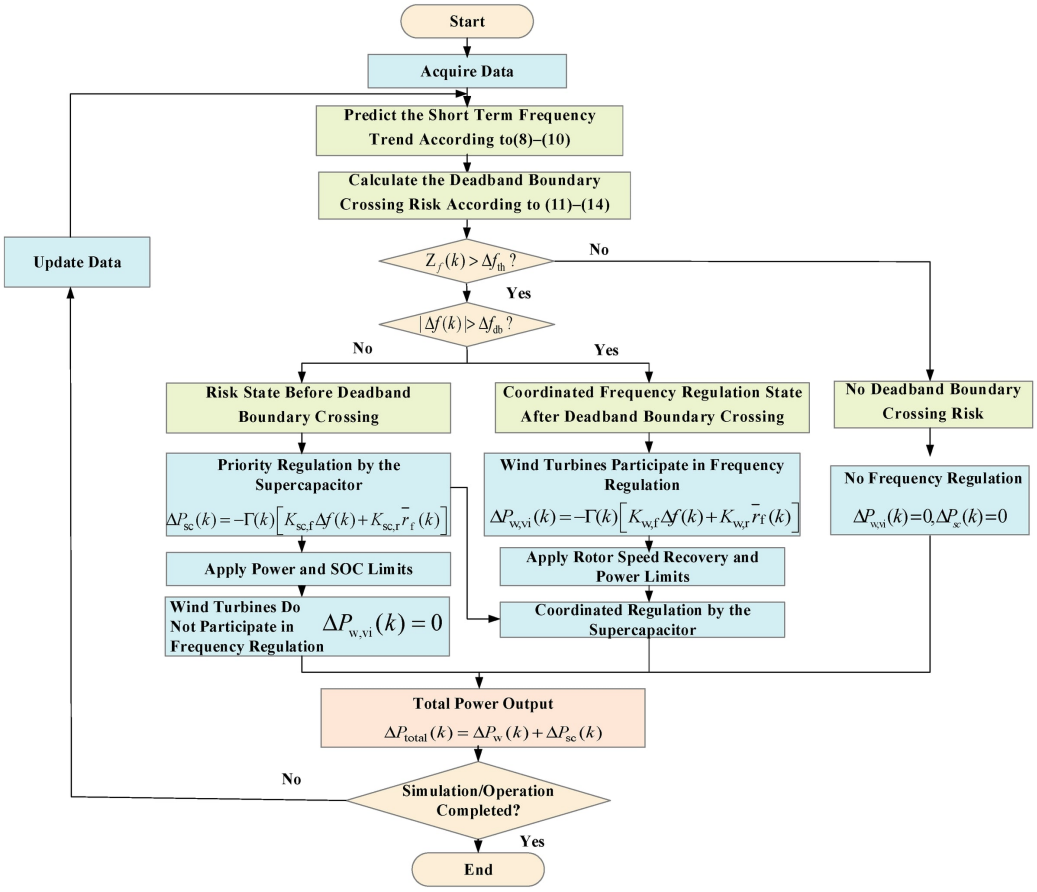


Figure 1. Procedure of the wind–storage coordinated frequency regulation control strategy.

5. Case Study

5.1. Case Study Setup

A case study is conducted on a modified IEEE 10-machine 39-bus system to verify the effectiveness of the proposed coordinated wind–storage frequency regulation strategy. The synchronous generator connected to bus 34 is replaced by an aggregated wind farm of equivalent capacity, and a supercapacitor energy storage system is connected to the same bus. The parameters of the wind farm and supercapacitor are listed in Table 2, while the parameters of the synchronous generators are set according to ref. [27]. The topology of the test system is shown in Figure 2.

The random power fluctuations of the wind farm over a 600-s period are used as the equivalent active power disturbance input to the system, as shown in Figure 3. The case study compares two frequency regulation strategies. Strategy 1, conventional coordinated wind–storage regulation, activates the wind farm and supercapacitor based on frequency deviation and RoCoF only after a PFR deadband boundary crossing, reflecting the passive response of conventional PFR. Strategy 2 activates only the supercapacitor for preemptive suppression when $Z_f(k) > \Delta f_{th}$ while the current frequency deviation remains within the PFR deadband. Once $|\Delta f(k)| > \Delta f_{db}$, the wind farm and supercapacitor provide coordinated frequency regulation subject to their respective operating constraints.

Table 2. Parameters of wind farm and supercapacitor energy storage system.

	Parameter	Value
Wind Farm	Rated Apparent Power Capacity	1000 MVA
	Inertia Time Constant	10 s
	Frequency Deviation Control Gain	20
	RoCoF Control Gain	8
	Rotor Speed Recovery Gain	0.2
	Initial Wind Speed	9.096 m/s
	Reference Output	508 MW
	Rotor-Speed Initial Point	11.052 rpm
Supercapacitor Energy Storage System	Rated Apparent Power Capacity	100 MVA
	Rated Energy Capacity	1 MWh
	Initial State of Charge	0.5
	SOC Range	[0.2, 0.8]
	Charging and Discharging Efficiency	95%
	Frequency Deviation Control Gain	20
	RoCoF Control Gain	8
	Specific Supercapacitor Investment Cost	70 million CNY/MWh
	Rated Cycle Life	1.0×10^6 cycles
	Deadband Width	0.033 HZ
	Warning Margin	0.01 HZ
	Prediction Horizon	0.3 s
	RoCoF Filter Coefficient	0.905
	Sampling Interval	0.02 s

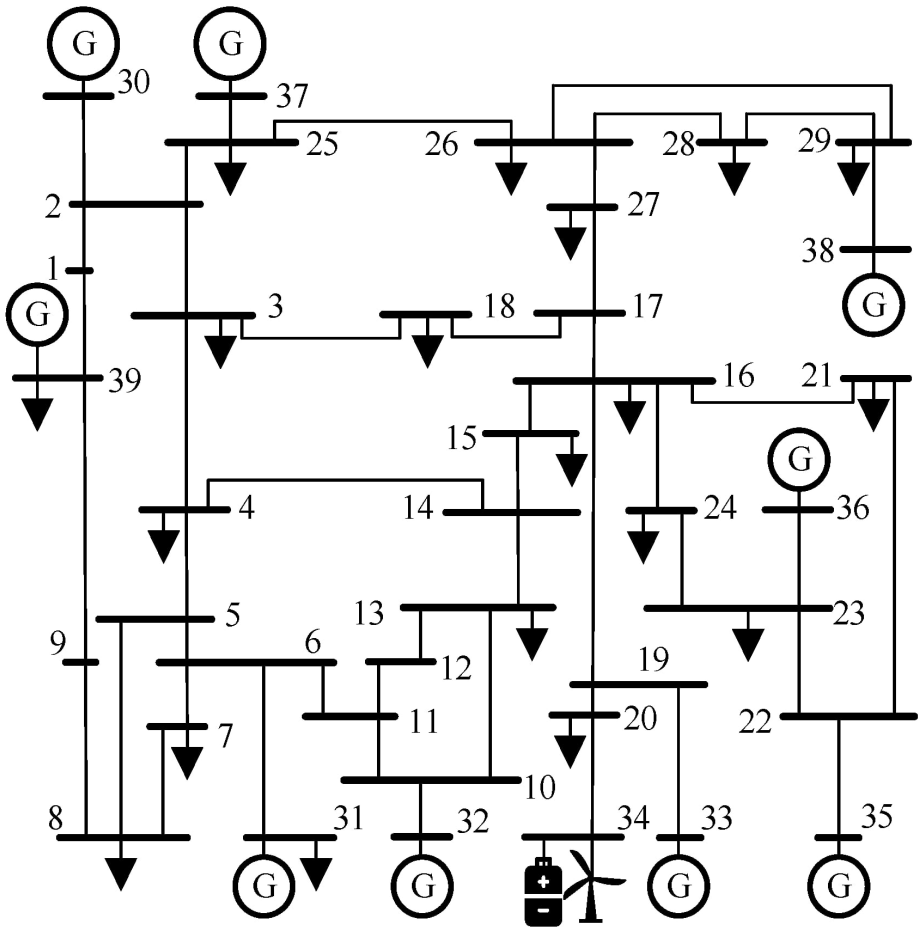


Figure 2. Topological diagram of the example system.

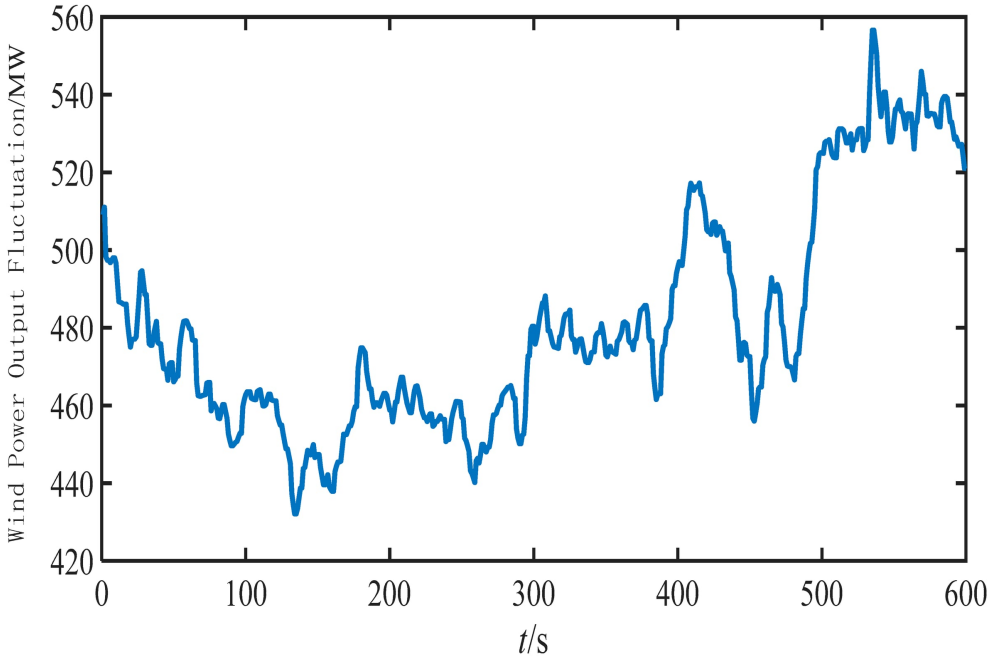


Figure 3. Wind power output fluctuation.

5.2. Comparison of Deadband Boundary Crossing Evaluation Metrics

Figure 4 compares the system frequency responses under the two frequency regulation strategies. Figures 5–7 compare the frequency regulation power provided by the thermal units, wind farm, and supercapacitor energy storage system, respectively. As shown by the frequency responses, the system frequency decreases and fluctuates following the disturbance under both strategies. With Strategy 1, the wind farm and supercapacitor participate in frequency regulation only after the frequency deviation crosses a deadband boundary. Consequently, pronounced frequency fluctuations occur near the deadband boundaries, resulting in repeated deadband boundary crossings. By contrast, Strategy 2 enables the supercapacitor to respond in advance at smaller frequency deviations and provide preemptive frequency support before the frequency deviation increases further. Therefore, the number of times that the frequency deviation crosses the deadband boundaries is significantly reduced, and the frequency fluctuations are effectively mitigated.

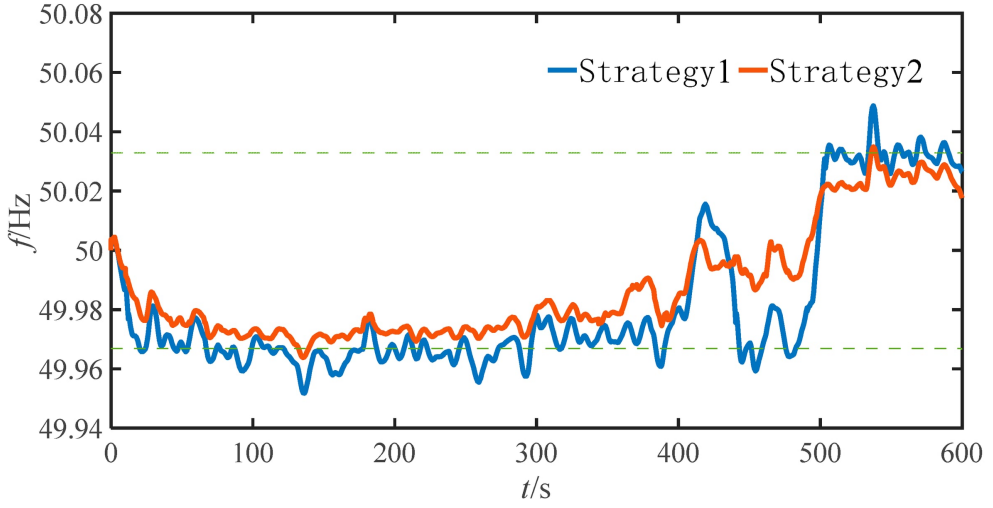


Figure 4. Comparison of frequency fluctuation curves.

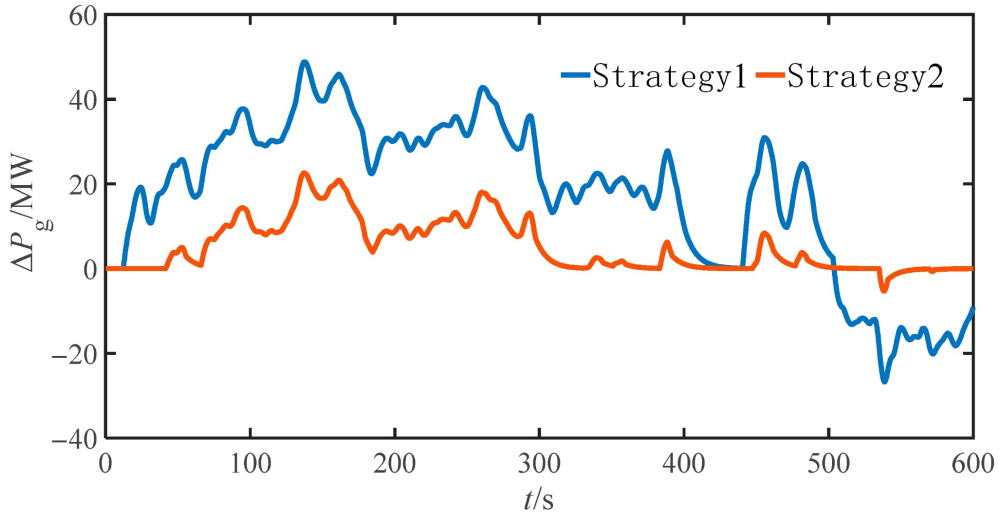


Figure 5. Comparison of frequency regulation power of thermal units.

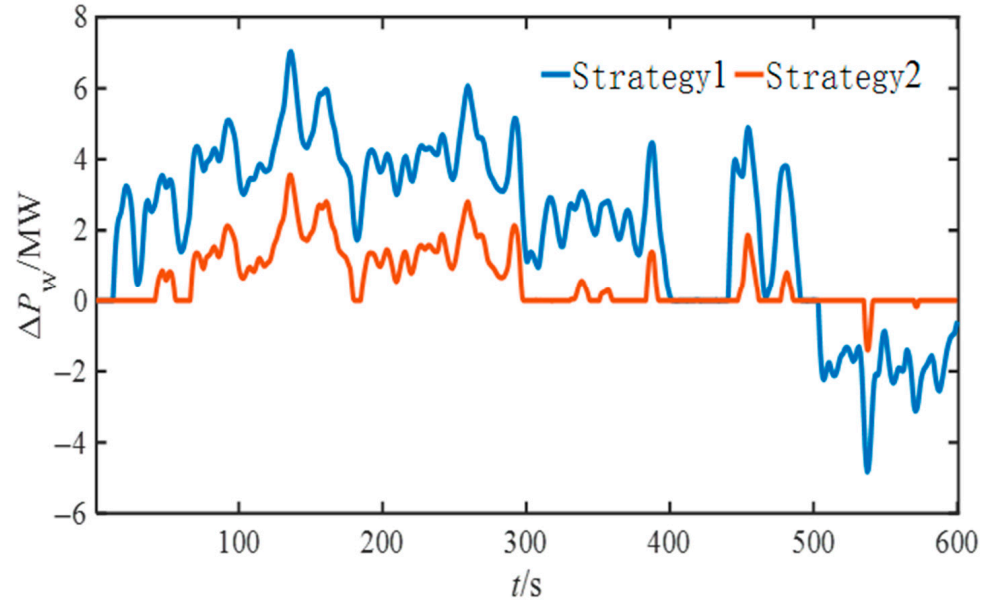


Figure 6. Comparison of frequency regulation power of wind power.

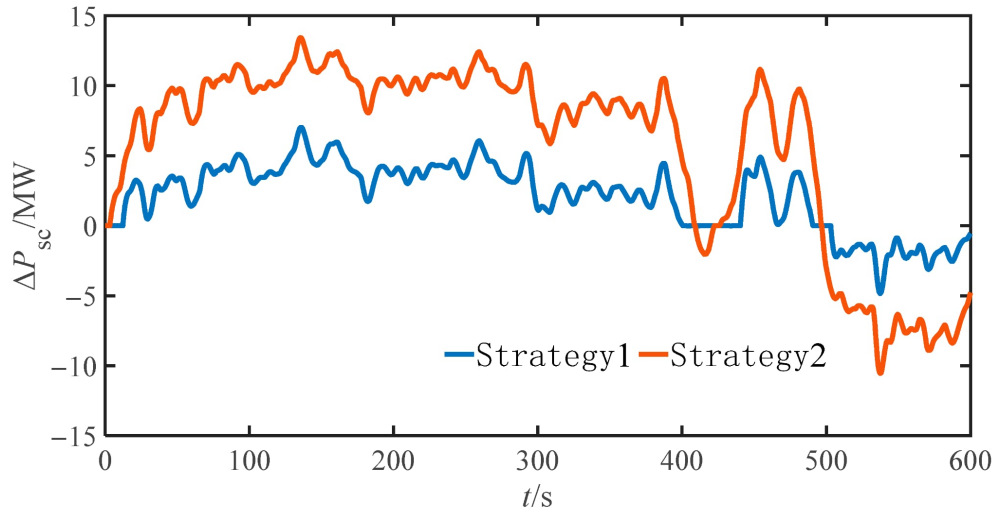


Figure 7. Comparison of frequency regulation power of supercapacitor.

Under Strategy 1, the thermal units and wind farm undergo relatively large changes in frequency regulation power, resulting in large output power fluctuations and strong regulating actions when the frequency deviation becomes large. Under Strategy 2, the overall magnitudes of the frequency regulation power provided by the thermal units and wind farm are significantly reduced, and their regulating actions are smoother during most periods. This demonstrates that the preemptive frequency regulation mechanism can redistribute the regulation burden as the frequency deviation develops.

The frequency regulation power response of the supercapacitor energy storage system further illustrates the control differences between the two strategies. Under Strategy 2, the supercapacitor participates in frequency regulation in advance at relatively small frequency deviations. It therefore exhibits a more proactive power response and provides power support during the early stage of the disturbance, thereby preventing the frequency from deviating further from its nominal value. Combined with the frequency responses, these results show that Strategy 2 suppresses the post-disturbance frequency deviation at an earlier stage through the fast response of the supercapacitor and the coordinated allocation of frequency regulation power among the supercapacitor, thermal units, and wind farm. Consequently, the number of deadband boundary crossings is reduced.

Table 3 presents the calculated deadband boundary crossing evaluation metrics for the two control strategies. As shown in the table, Strategy 2 achieves better suppression of deadband boundary crossings than Strategy 1. Specifically, the maximum deadband exceedance magnitude is reduced by 0.0126 Hz, the deadband boundary crossing count is reduced by 25, and the deadband boundary switching intensity is reduced by approximately 92.59%. This improvement is achieved because the proposed strategy uses the supercapacitor for preemptive suppression when the frequency deviation has not yet crossed a PFR deadband boundary. Under the proposed activation logic, the supercapacitor responds preemptively when the combined frequency risk magnitude exceeds the warning threshold while the current frequency deviation remains within the deadband. Wind turbine frequency support is enabled only after actual deadband exceedance. This effectively reduces repeated deadband boundary crossings. Once the frequency deviation crosses a deadband boundary, the wind farm and supercapacitor jointly participate in frequency regulation, further limiting the increase in frequency deviation. Therefore, Strategy 2 not only reduces the maximum deadband exceedance magnitude but also significantly decreases the deadband boundary crossing count and deadband boundary switching intensity, demonstrating superior suppression of deadband boundary crossings and improved frequency regulation performance.

Table 3. Evaluation metrics for deadband boundary crossing corresponding to the two strategies.

	A_{db}^{max} /Hz	N_{db}	S_{db}	MAE/Hz	RMSE/Hz
Strategy 1	0.0158	27	54	0.0299	0.0311
Strategy 2	0.0032	2	4	0.0211	0.0228

The present case study evaluates the closed-loop performance of the coordinated controller. It does not independently quantify the forecasting error, warning lead time, or false-alarm and missed-event rates of the risk activation method. Such an assessment would require explicit event definitions, temporal matching rules, and suitable reference trajectories that account for the effect of control intervention.

5.3. Four-Strategy Ablation Study

To examine the effects of the individual control mechanisms on the frequency response, four control strategies are compared under identical simulation conditions. Strategy 1 is the conventional coordinated regulation strategy in which the wind farm and supercapacitor participate after a deadband boundary crossing. Strategy 2 is the proposed risk-prediction strategy: the supercapacitor participates preemptively according to the risk activation coefficient $\Gamma(k)$ during the deadband-crossing risk stage, and the wind farm and supercapacitor provide coordinated regulation after a boundary crossing. Strategy 3 does not include the supercapacitor, and the wind farm participates only after the frequency crosses a deadband boundary. Strategy 4 determines the pre-crossing participation of the supercapacitor using the current frequency deviation and a fixed warning threshold, without using the short-term predicted frequency or the normalized crossing-risk index; its post-crossing control law and resource limits are identical to those of Strategy 1. The frequency response curve is shown in Figure 8.

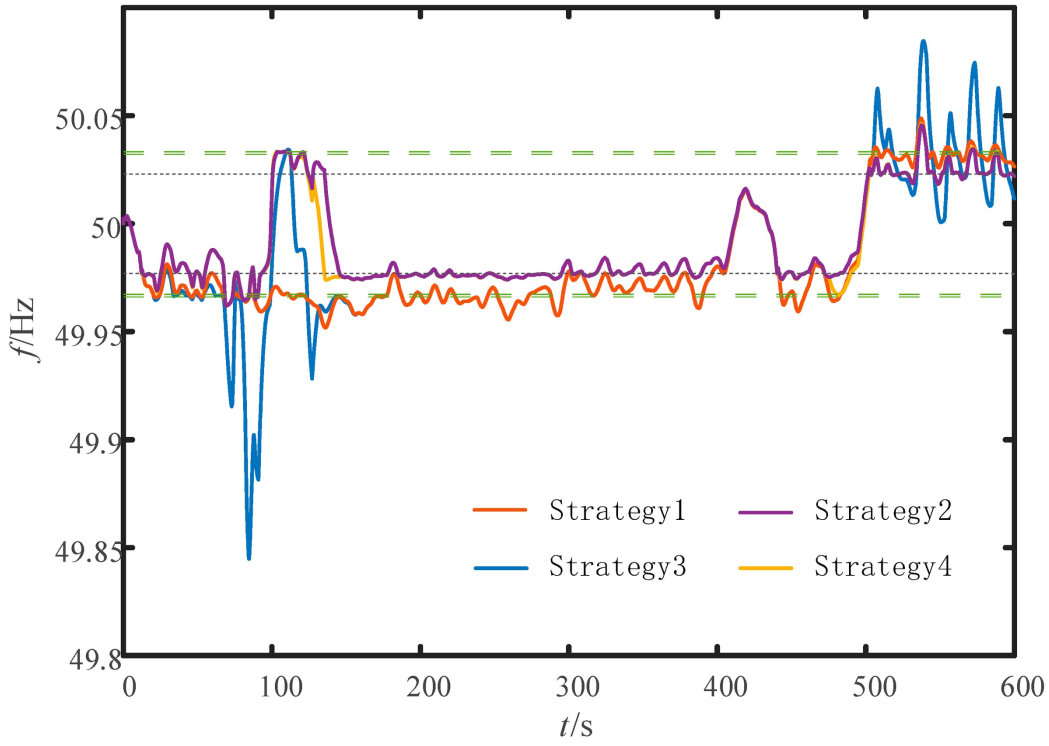


Figure 8. Frequency responses under four strategies.

Table 4 presents the frequency evaluation results of the four strategies under the same representative disturbance. Comparing Strategies 3 and 1, the inclusion of the supercapacitor reduces the maximum deadband exceedance magnitude from 0.1222 Hz to 0.0162 Hz, while MAE and RMSE decrease from 0.0319 Hz and 0.0366 Hz to 0.0302 Hz and 0.0341 Hz, respectively. The crossing count changes from 24 to 30 for this trajectory, indicating that error magnitude and crossing count characterize different aspects of the frequency response. Compared with Strategy 1, Strategy 4 reduces the crossing count from 30 to 8 and MAE from 0.0302 Hz to 0.0223 Hz. Relative to Strategy 4, Strategy 2 further reduces MAE and RMSE to 0.0220 Hz and 0.0230 Hz, respectively, and reduces the crossing count from 8 to 7. These results illustrate the respective effects of the supercapacitor, preemptive participation, and risk prediction for the representative trajectory.

Table 4. Comprehensive Performance Comparison of Four Frequency Regulation Strategies in the Ablation Study.

	A_{db}^{max} /Hz	N_{db}	S_{db}	MAE/Hz	RMSE/Hz
Strategy 1	0.0162	30	60	0.0302	0.0341
Strategy 2	0.0125	7	14	0.0220	0.0230
Strategy 3	0.1222	24	48	0.0319	0.0366
Strategy 4	0.0132	8	16	0.0223	0.0233

The comparison between Strategies 3 and 1 assesses the effect of supercapacitor participation under post-crossing regulation. The comparison between Strategies 1 and 4 assesses preemptive supercapacitor support using a fixed warning threshold. The comparison between Strategies 4 and 2 assesses the combined contribution of short-term prediction and the risk index relative to fixed-threshold activation. Because prediction and risk-index use are changed together in the last comparison, their individual contributions are not separately identified. Within the evaluated conditions, pre-crossing support provides the main reduction in repeated boundary crossings, while the combined prediction and risk-index mechanism provides smaller additional improvements in frequency error.

5.4. Multi-Scenario and Statistical Robustness Analysis

Four additional disturbance scenarios—load increase, load decrease, wind-power drop, and wind gust—are considered, and the four strategies are compared using 100 paired random realizations.

Table 5 reports the mean metrics across the 100 realizations. Strategy 1 reduces the maximum deadband exceedance magnitude, MAE, and RMSE compared with Strategy 3, Strategy 4 reduces the mean crossing count from 115.36 to 17.78, compared with Strategy 1, and Strategy 2 further reduces MAE and RMSE to 0.0354 Hz and 0.0418 Hz. The responses show that pre-crossing support delays the first crossing and reduces repeated switching near the boundary. Under sustained power imbalances, however, finite storage capacity also affects the subsequent frequency peak; a lower crossing count therefore does not always accompany a lower peak deviation. Values are sample means across 100 realizations. $A_{\mathrm{db}}^{\max}$ is the average of the maximum deadband exceedance obtained in each realization; N_{db} and S_{db} are the mean crossing count and switching intensity.

Table 5. Mean evaluation metrics across 100 paired realizations.

	A_{db}^{max} /Hz	N_{db}	S_{db}	MAE/Hz	RMSE/Hz
Strategy 1	0.1114	115.36	230.12	0.0371	0.0429
Strategy 2	0.1118	17.37	34.34	0.0354	0.0418
Strategy 3	0.1352	22.97	45.29	0.0426	0.0501
Strategy 4	0.1117	17.78	35.16	0.0357	0.0420

The multi-scenario, noise, and parameter-sensitivity results show that pre-crossing supercapacitor participation primarily improves switching characteristics near the deadband boundaries, while short-term prediction and the risk index provide smaller reductions in average frequency error. MAE and RMSE are reduced within the tested parameter combinations, whereas crossing count and maximum exceedance are more dependent on the disturbance and measurement noise. These findings support allocating short-term regulation duties according to the response characteristics of the wind turbine and super-

capacitor, with performance assessed using the available resource energy and multiple frequency metrics.

5.5. Comparison of Overall Operating Costs

The proposed strategy reduces the frequency regulation actions of the wind turbines and thermal units by increasing those of the supercapacitor energy storage system. To assess the economic justification of its preemptive activation, an overall operating cost is introduced, including the frequency regulation loss costs of the supercapacitor, thermal units, and wind farm, as well as the loss of generation revenue caused by the wind farm operating away from its MPPT point.

During frequency regulation, the supercapacitor undergoes frequent charging and discharging, often with shallow variations in its state of charge. To estimate its cycling-related degradation cost, the rainflow-counting method is applied to the supercapacitor SOC trajectory. Each full cycle is counted as one cycle, and each half cycle as one-half cycle. For the simplified cost assessment in this study, the degradation per counted cycle is assumed to be independent of cycle depth within the specified SOC range. The resulting cycle count is normalized by the rated cycle life to estimate the degradation cost, as given in (28).

$$N_{\mathrm{sc,rf}} = N_{\mathrm{full}} + \frac{1}{2}N_{\mathrm{half}}, \quad C_{\mathrm{sc}} = C_{\mathrm{sc,inv}}\frac{N_{\mathrm{sc,rf}}}{N_{\mathrm{sc,life}}} \tag{28}$$

where $C_{\mathrm{sc,inv}}$ is the total investment cost of the supercapacitor system; C_{sc} denotes the supercapacitor degradation cost accumulated over the simulation period, in CNY; $N_{\mathrm{sc,rf}}$ is the rainflow-counted cycle number, with N_{full} and N_{half} denoting the numbers of full and half cycles, respectively; and $N_{\mathrm{sc,life}}$ is the rated cycle life of the supercapacitor.

During frequency regulation, the governors and steam-turbine valves of thermal units are adjusted frequently, resulting in additional operating wear and losses. An equivalent cost model based on the frequency regulation power and its variation is adopted to quantify the losses associated with frequency regulation by thermal units.

$$C_{\mathrm{th}} = \sum_{i=1}^{N_{\mathrm{th}}} c_{\mathrm{th}} \sum_{k=2}^{N} \left|\Delta P_{\mathrm{th},i}(k) - \Delta P_{\mathrm{th},i}(k-1)\right| \tag{29}$$

where Nth is the number of thermal units participating in frequency regulation; $\Delta P_{\mathrm{th},i}(k)$ is the frequency regulation power of the i thermal unit at the k sampling instant; and cth is the unit cost of frequency regulation losses for thermal units.

Wind turbines provide supplementary active-power support by adjusting their output and rotor speed. The wind-regulation cost in the economic comparison represents the power-variation-related regulation burden under the adopted model. Its implications for component fatigue and turbine service life can be further evaluated through turbine-level torque and load analysis.

$$C_{\mathrm{w}} = \sum_{i=1}^{N_{\mathrm{w}}} c_{\mathrm{w}} \sum_{k=2}^{N} \left|\Delta P_{\mathrm{w},i}(k) - \Delta P_{\mathrm{w},i}(k-1)\right| \tag{30}$$

where N_{w} is the number of wind turbines participating in frequency regulation; $\Delta P\mathrm{w,i(k)}$ is the frequency regulation power of wind turbine i at sampling instant k; and c_{w} is the unit cost of frequency regulation losses for wind turbines.

When a wind turbine participates in system frequency regulation, its actual active power delivered to the grid deviates from the MPPT operating point, resulting in a loss of wind energy production. This loss can be calculated as the product of the reduction in

energy production caused by operation away from the MPPT point and the wind power feed-in tariff.

$$C_{\mathrm{w,MPPT}} = \lambda_{\mathrm{w}} \sum_{i=1}^{N_{\mathrm{w}}} \sum_{k=1}^{N} \Delta P_{\mathrm{loss},i}(k) \frac{\Delta t}{3600} \tag{31}$$

where λ_{w} is the wind power feed-in tariff. $\Delta P_{\mathrm{loss},i}(k)$ is determined from Equation (16) or Equation (18), according to the regulation direction and rotor-speed state of the ith wind turbine at time k.

The overall operating cost is the sum of the frequency regulation loss costs of the supercapacitor, thermal units, and wind turbines, as well as the loss of wind power generation revenue.

$$C_{\mathrm{total}} = C_{\mathrm{sc}} + C_{\mathrm{th}} + C_{\mathrm{w}} + C_{\mathrm{w,MPPT}} \tag{32}$$

Table 6 presents the modeled operating costs of the two strategies. Strategy 1 adopts the conventional wind–storage regulation scheme, in which the wind farm and supercapacitor respond after a deadband crossing. Its supercapacitor cycling cost is CNY 140.00, while its thermal-regulation, wind-regulation, and MPPT-loss costs are CNY 71.20, CNY 21.40, and CNY 216.77, respectively. Under Strategy 2, the supercapacitor is activated in advance when the frequency enters the warning region and continues to move toward the deadband boundary. The corresponding costs are CNY 70.00, CNY 70.91, CNY 19.19, and CNY 214.79. Thus, the calculated supercapacitor cycling cost is lower under Strategy 2, and the other three cost components also decrease, although their reductions are comparatively small. The reduction in the wind-regulation cost term reflects a lower power-variation-related cost under the adopted model; its implications for turbine fatigue life require further assessment using turbine-level torque and load data.

Table 6. The overall operating cost corresponding to the two strategies.

	Strategy 1	**Strategy 2**
$N_{\mathrm{sc,rf}}$	2	1
C_{sc}/CNY	140	70
Cth/CNY	71.2	70.91
C_{w}/CNY	21.4	19.19
$C_{\mathrm{w,MPPT}}$/CNY	216.77	214.79
C_{total}/CNY	449.36	374.88

The total modeled costs of Strategies 1 and 2 are CNY 449.36 and CNY 374.88, respectively. Strategy 2 therefore reduces the modeled cost by CNY 74.48. The supercapacitor cycling cost accounts for CNY 70.00 of this difference, approximately 94% of the total; the thermal-regulation, wind-regulation, and MPPT-loss costs together account for the remaining CNY 4.48. The lower cost in this case is consequently driven mainly by the change in the counted supercapacitor cycles, rather than by a substantial reduction in wind- or thermal-regulation costs. Compared with Strategy 1, Strategy 2 reduces the overall operating cost by 16.57%. These results indicate that the proposed strategy improves frequency quality while achieving a reasonable allocation of the frequency regulation burden among different resources, thereby providing an advantage in terms of overall operating cost.

6. Conclusions

To address the frequent activation of frequency regulation resources, deterioration of frequency quality, and increased operating costs caused by repeated PFR deadband boundary crossings, this paper proposes a coordinated frequency regulation strategy for wind power and energy storage to suppress frequency fluctuations. The proposed method

predicts the risk of deadband boundary crossing based on the frequency deviation, RoCoF, and frequency predictions over a short time horizon. It then implements hierarchical coordinated regulation according to the response characteristics of the supercapacitor energy storage system and wind turbines. The following conclusions are drawn from the case study:

(1) The proposed strategy can effectively identify the risk of deadband boundary crossing as the frequency approaches a PFR deadband boundary. It then activates the supercapacitor energy storage system in advance to rapidly suppress frequency fluctuations over a short time scale. Compared with the conventional control strategy, the proposed strategy reduces repeated deadband boundary crossings, the deadband exceedance magnitude, and the deadband boundary switching intensity, thereby improving system frequency quality.

(2) Under the case-study settings, Strategy 2 achieves a lower modeled total cost, with most of the reduction arising from the supercapacitor cycling-cost term. The wind-regulation cost term also decreases, reflecting a lower power-variation-related cost under the adopted model. By assigning rapid, short-duration fluctuations primarily to the supercapacitor, the proposed strategy reduces repeated short-term adjustments by wind turbines and may help moderate dynamic loading. The implications for turbine fatigue and service life warrant further assessment using turbine-level torque, load, and fatigue analyses.

Author Contributions: Conceptualization, K.L. and C.L.; methodology, R.S. and Y.L.; validation, X.Z. and M.Z.; formal analysis, R.S.; data curation, J.D. and T.Y.; writing—original draft preparation, R.S.; writing—review and editing, K.L.; visualization, Z.T. and C.L.; supervision, J.D. and X.Z.; project administration, Z.T.; funding acquisition, M.Z. All authors have read and agreed to the published version of the manuscript.

Funding: This research was funded by the NorthEast Branch of State Grid Corporation of China, grant number SGDB0000GHJS2500584.

Data Availability Statement: The datasets presented in this article are not readily available because the data are part of an ongoing study and due to technical time limitations.

Acknowledgments: The authors gratefully acknowledge the financial and data support provided by the NorthEast Branch of State Grid Corporation of China.

Conflicts of Interest: Author Rui Sun and Kexin Li was employed by the company NorthEast Branch of State Grid Corporation of China. The remaining authors declare that the research was conducted in the absence of any commercialor financial relationships that could be construed as a potential conflict of interest. The authors declare that this study received funding from NorthEast Branch of State Grid Corporation of China. The funder had the following involvement with the study: Conceptualization, Data curation, Investigation, study design.

References

1. Mohandes, B.; El Moursi, M.S.; Hatziargyriou, N.; El Khatib, S. A review of power system flexibility with high penetration of renewables. *IEEE Trans. Power Syst.* **2019**, *34*, 3140–3155. [CrossRef]
2. Impram, S.; Nese, S.V.; Oral, B. Challenges of renewable energy penetration on power system flexibility: A survey. *Energy Strategy Rev.* **2020**, *31*, 100539. [CrossRef]
3. Li, Z.; Cheng, Z.; Liang, J.; Si, J. Distributed cooperative AGC method for new power system with heterogeneous frequency regulation resources. *IEEE Trans. Power Syst.* **2023**, *38*, 4928–4939. [CrossRef]
4. Xiong, W.; Yan, F.; Wang, Y.; Luo, S.; Chen, W.; Chen, L. Analysis on variation of frequency probability distribution and causes in actual power grid. *Autom. Electr. Power Syst.* **2020**, *44*, 222–227.
5. Jiang, S.; Zheng, S.; Li, G.; Xin, Y.; Wang, L.; Wang, T. Adaptive coordinated control strategy of frequency active support for MMC-HVDC systems considering frequency regulation dead zone. *Proc. CSEE* **2025**, *45*, 7893–7905.
6. An, J.; Li, K.; Zhou, Y.; Tang, W.; Shi, Y. Frequency fluctuation suppression-oriented evaluation of frequency regulation capability requirements for new-type power systems. *Trans. China Electrotech. Soc.* **2026**, *41*, 1495–1509.

7. Liu, J.; An, B.; Liu, G.; Zhang, W.; Ma, C.; Ge, L. Research on remaining service life prediction of wind turbine bearings. *Acta Energiae Solaris Sin*. **2025**, *46*, 589–595.
8. Hu, D.; Dai, X.; Ren, J.; Li, W.; Xu, Y.; Chen, H. Research progress on flywheel energy storage and rotor fatigue life analysis. *Adv. Technol. Electr. Eng. Energy* **2025**, *44*, 136–148.
9. Lim, S.; Kim, T.; Lee, K.Y.; Choi, D.; Park, J.-W. Impact of high penetration of renewables on power system frequency response: A review and verification. *Renew. Sustain. Energy Rev.* **2025**, *217*, 115728. [CrossRef]
10. Saleem, M.I.; Saha, S. Assessment of frequency stability and required inertial support for power grids with high penetration of renewable energy sources. *Electr. Power Syst. Res.* **2024**, *229*, 110184. [CrossRef]
11. Saha, S.; Saleem, M.; Roy, T. Impact of high penetration of renewable energy sources on grid frequency behaviour. *Int. J. Electr. Power Energy Syst.* **2023**, *145*, 108701. [CrossRef]
12. Kheshti, M.; Lin, S.; Zhao, X.; Ding, L.; Yin, M.; Terzija, V. Gaussian distribution-based inertial control of wind turbine generators for fast frequency response in low inertia systems. *IEEE Trans. Sustain. Energy* **2022**, *13*, 1641–1653. [CrossRef]
13. Vidyanandan, K.V.; Senroy, N. Primary frequency regulation by deloaded wind turbines using variable droop. *IEEE Trans. Power Syst.* **2013**, *28*, 837–846. [CrossRef]
14. Tian, S.; Liu, Y.; Tian, X.; Li, B.; Chi, Y. A wind farm control strategy for frequency regulation reserve: Optimize wake loss and frequency support capability. *Renew. Energy* **2024**, *237*, 121645. [CrossRef]
15. Prasad, R.; Padhy, N.P. Synergistic frequency regulation control mechanism for DFIG wind turbines with optimal pitch dynamics. *IEEE Trans. Power Syst.* **2020**, *35*, 3181–3191. [CrossRef]
16. Hu, Z.; Gao, B.; Zhang, L.; Wang, W.; Pan, S. Bidirectional support capability analysis and adaptive inertial control strategy of wind turbine. *Trans. China Electrotech. Soc.* **2023**, *38*, 5224–5240.
17. Li, K.; An, J.; Shi, Y.; Zhou, Y.; Liu, C. An integrated virtual inertia control parameter setting method for wind turbine based on available frequency regulation energy. *Trans. China Electrotech. Soc.* **2025**, *40*, 1382–1394.
18. Zhang, F.; Li, B.; Ding, L. Parameter setting method of time-varing frequency regulation considering linked energy distribution of wind power for frequency regulation. *Autom. Electr. Power Syst.* **2022**, *46*, 188–197.
19. Afshar, Z.; Bhogaraju, I.; Rahmanei, H.; Farasat, M. Hierarchical frequency and SOC control of power grids with battery energy storage systems. *IEEE Trans. Power Electron.* **2024**, *39*, 7925–7937. [CrossRef]
20. Zhao, T.; Parisio, A.; Milanovic, J.V. Distributed control of battery energy storage systems for improved frequency regulation. *IEEE Trans. Power Syst.* **2020**, *35*, 3729–3738. [CrossRef]
21. He, G.; Chen, Q.; Kang, C.; Xia, Q.; Poolla, K. Cooperation of wind power and battery storage to provide frequency regulation in power markets. *IEEE Trans. Power Syst.* **2017**, *32*, 3559–3568. [CrossRef]
22. Pei, M.; Wang, Q.; Ye, L.; Luo, Y.; Sha, L.; Zhang, Z.; Song, X. Hierarchical control strategy of wind-storage frequency support for SOC recovery optimization and arbitrage revenue. *Appl. Energy* **2024**, *365*, 123229. [CrossRef]
23. Shu, H.; Wang, G.; Chen, J.; Ma, H.; He, T. Coordinated control of wind-storage combined with primary frequency regulation and variable coefficient based on wind speed and SOC. *J. Energy Storage* **2024**, *87*, 111356. [CrossRef]
24. Rashid, L.B.; Rehman, S.; Zayed, M.E.; Ibrahim, R.; Drammeh, F.; Shalaby, S.M.; Mujtaba, I.M. Empowering Wind Energy Output Optimization: Comparative Assessment of Hybrid Artificial Intelligence Mod-els Towards Wind Speed Forecasting Accuracy. *Energies* **2026**, *19*, 4159. [CrossRef]
25. Zhang, W.; Sun, C.; Wang, Y.; Song, K. A novel voltage-power coordinated control strategy for grid-connected inverters in low-voltage microgrids based on fast non-singular terminal sliding mode. *Electr. Power Syst. Res.* **2026**, *251*, 112183. [CrossRef]
26. Zhang, W.Q.; Sun, C.; Zeng, Y.; Hasanien, H.M.; Wang, Y. Design and dynamic characteristic analysis of NTSM with variable gains for full-parameter perturbation systems: A case of DC-DC converters. *ISA Trans.* **2026**, *172*, 364–384. [CrossRef]
27. Huang, Z.; Zhang, X.; Li, G.; Li, J.; Tian, X. Transient frequency regulation strategy for battery energy storage system based on frequency regulation characteristic compensation. *Trans. China Electrotech. Soc.* **2026**, *41*, 2949–2962.

Disclaimer/Publisher's Note: The statements, opinions and data contained in all publications are solely those of the individual author(s) and contributor(s) and not of MDPI and/or the editor(s). MDPI and/or the editor(s) disclaim responsibility for any injury to people or property resulting from any ideas, methods, instructions or products referred to in the content.